Ceramics International 48 (2022) 931–940

Contents lists available at ScienceDirect

Ceramics International

journal homepage: www.elsevier.com/locate/ceramint

Synthesis and multiferroic properties of particulate composites resulting from combined size effects of the magnetic and ferroelectric phases

Diego Seiti Fukano Viana [a,*], Adilson Jesus Aparecido De Oliveira [a], Korllvary Rhanddy Charles Parra Jimenez [a], Flavio Paulo Milton [a], José Antonio Eiras [a], Guilherme Maia Santos [b], Ducinei Garcia [a]

[a] Physics Department, Federal University of São Carlos, Rod. Washington Luís, km 235 - SP-310, São Carlos, SP, 13565905, Brazil
[b] Physics Department, State University of Maringá, Av. Colombo, 5790 - Zona 07, Maringá, PR, 87020-900, Brazil

ARTICLE INFO

Keywords:
Ferroelectric properties
Magnetic properties
Grain size
Composites
Multiferroics

ABSTRACT

The effect of grain size was not fully explored in composites containing ferroelectric and magnetic phases including the independent properties of each phase. Aiming to study the dependence of ferroic and multiferroic properties with average grain size in composites this work reports preparation method and electric, magnetic and magnetoelectric properties of particulate composites with distinct combination of grain size of each phase. A new sintering method was applied to prepare a group of samples with distinct configuration of grain size distribution. With this method it was possible to densify ceramics avoiding grain growth using spark plasma sintering. It was observed that the all ferroic and multiferroic properties were correlated with the setup of grain size of each phase in the composite, by example the dependence of magnetic properties with the electric phase grain size. Besides it was noticed that is possible to improve magnetoelectric coefficient by changing grain size of both phase, even inducing the self-biased effect by decreasing the grain size of the ferroelectric phase.

1. Introduction

The development of multifunctional materials to be applied in sensors and actuators have been facing many challenges, besides of the multifunctional features, the performance as well as the reduction to the nanometric scale [1,2]. By example, multifunctional materials holding more than one ferroic order simultaneously, such as the magnetic and electric order, could be applied in devices where the coupling of these orders, magnetoelectric effect, can be exploited [3]. There is already a wide range of possible applications for these materials, for example, ac and dc magnetic field sensors, multi-state memories, solar cells, etc. [4,5].

In composite materials the coupling between magnetic and electric properties is given by mechanical deformation induced by application of an external signal (i.e., piezoelectric by applying an electric field or magnetostrictive by application of magnetic field). From the point of view of magnetoelectric coefficient, studies have pointed out several factors which affect it, such as magnetic/piezoelectric phase performance; degree of connectivity; the average grain size of each phase; among others [1]. In this sense, such factors should be considered when choosing the design of the material (composition) and processing technique [1].

Studies have shown an anomalous behavior on the dependence of the magnetoelectric coefficient (MC) with the magnetic field in composite materials characterized by a spontaneous response in MC at null bias magnetic field, called self-biased effect (SB) [6–8]. One of the origins of this effect, as observed in heterostructure, is related to intrinsic mechanical stress inherent to interfaces of distinct phases [6]. Since the strain could be generated by lattice mismatch and thermal expansion mismatch between different constituents [6], downsizing the grain size is a way to induce self-biased effect by mechanical stress. By the other side, increasing or decreasing the grain size will not only result on change MC, but also it will bring consequences on the electric and magnetic properties.

The effect of reducing the average grain size of ferroelectrics on the piezoelectric, dielectric and ferroelectric properties has been studied [9–11] and it was reported the decrease of these properties with downsizing the grain size [1]. Besides, a structural transition from tetragonal to monoclinic or cubic structure driven by reduction of grain size was already reported for (x) $[PbMg_{1/3}Nb_{2/3}O_3]$ – (1-x) $[PbTiO_3]$ for

* Corresponding author. Physics Department, Washington Luís Highway, 235 km - SP-310, São Carlos, São Paulo, 13565-905, Brazil.
E-mail address: diegos@uftpr.edu.br (D.S.F. Viana).

https://doi.org/10.1016/j.ceramint.2021.09.177
Received 9 July 2021; Received in revised form 28 August 2021; Accepted 16 September 2021
Available online 24 September 2021

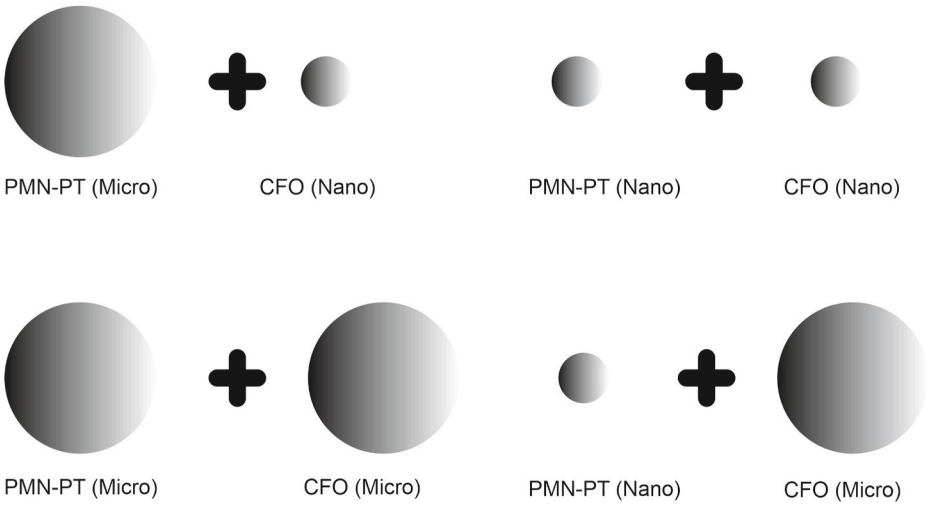

Fig. 1. Flowchart of powder combination of PMN-PT and CFO. Nomenclature (nano) and (micro) refers to the order of magnitude of the average particle size.

Table 1
Sintering temperature, grain size and electric field applied for electric polarization for samples thermal treated for 24 h. Values of electrical resistivity and apparent density dependence with thermal treatment time (for 0 h and 36 h the grain size and applied electric field for electric polarization were not measured).

Sample Electric (E) Magnetic (M)	Grain Size Average (nm)	Sintering Temperature (^{0}C)	Poling electric Field (kV/mm)	Electric Resistivity (Ω.m)			Apparent Density (g/cm^3)		
				Duration of Thermal Treatment					
				0 h	24 h	36 h	0 h	24 h	36 h
E (nano)	230	800	2	$1.7x10^2$	$4.4x10^7$	$4.4x10^6$	6.2	7.3	7.2
M(nano)	250								
E (nano)	260	800	2	$1.8x10^3$	$3.7x10^6$	–	6.3	6.7	–
M (micro)	1000								
E (micro)	1600	900	0.8	$6.6\ x10^2$	$3.8x10^6$	$1.2x10^6$	7.5	7.7	7.4
M (nano)	250								
E (micro)	1600	950	0.3	$1.8\ x10^2$	$1.1x10^6$	$9.2x10^4$	7.6	7.7	7.5
M (micro)	1000								

many compositions [12,13].

$CoFe_2O_4$ (CFO) saturation magnetization, coercive field and remanent magnetization are related with several variables such as grain size, degree of oxidation of iron and cobalt, grain morphology, among others [14–17]. In addition, studies have shown increase in magnetization increasing the grain size [18]. In polycrystalline materials, coercive field exhibits an inverse dependence on grain size [19], besides according Cullity [20], in the case of materials with magnetic multidomains the value coercive field are inversely proportional of grain size.

It has been shown that the downsizing of the ferroelectric phase in magnetoelectric composites decrease the magnetoelectric effect due the reduction of ferroelectric, dielectric and piezoelectric response [1,21]. According simulations from Yue et al. [22], when a piezoelectric material (PZT or $BaTiO_3$) is used as composite matrix, ME effect gradually becomes weaker as the internal length scale of the piezoelectric matrix is decreasing. In contrast, the magnetoelectric effect is enhanced when the internal length scale of the piezomagnetic inhomogeneity ($CoFe_2O_4$) is decreasing. In composites containing 80 mol% of (0.675) $[PbMg_{1/3}Nb_{2/3}O_3]$ – (0.325) $[PbTiO_3]$ (PMN-PT) and 20 mol% $CoFe_2O_4$ (CFO) it was observed the influence of stress generated by decrease of temperature in magnetoelectric response, at 300 K an ordinary magnetoelectric coefficient behavior was obtained meanwhile at 5 K a hysteric behavior was noticed [23]. Since grain size could change mechanical interaction between the phases [24,25], the effect of decreasing temperature on magnetoelectric coefficient observed by Gualdi et al. [23] could be induced at room temperature by changing the grain size of both phases.

To obtain ceramics with controlled grain size is necessary a densification technique which prevents grain growth of powders with small particle size. Conventional sintering often leads to grain growth providing dense but coarsened grained ceramics, due to the high temperatures applied for densification [26,27]. There are several methods reported which could be applied to densify ceramics, however the spark plasma sintering (SPS) has clear advantages over conventional sintering methods, making possible to sinter nanometric powders to near full densification with little grain growth and avoid reaction between the compounds of the composite [26].

Aiming to study the dependence of ferroic and multiferroic properties with the combined size effects of both phases this work reports the preparation method and electric, magnetic and magnetoelectric properties of particulate composites of (0.675) $[PbMg_{1/3}Nb_{2/3}O_3]$ – (0.325) $[PbTiO_3]$ (PMN-PT) and $CoFe_2O_4$ (CFO).

2. Experimental

Magnetoelectric composites of 0.675 $[PbMg_{1/3}Nb_{2/3}O_3]$ – 0.325 $[PbTiO_3]$ (PMN-PT) and $CoFe_2O_4$ (CFO) were prepared by the solid-state reaction method. The cobalt ferrite powder was prepared using Co_3O_4 and Fe_2O_3 as starting materials. The powders were mixed through ball milling (in distilled water with ZrO_2 cylinders), calcined at 900 °C, for 4 h, and then, grinded (again by ball milling), for 10 h. Aiming the increase the particle size an additional thermal treatment was applied, 1100 °C for 4 h.

PMN-PT powder, with nominal formula (1-x) (Pb $(Mg_{1/3}Nb_{2/3})O_3$ – (x) $PbTiO_3$ (x = 0.325), was obtained by the Columbite Method. The columbite precursor, $MgNbO_6$ (MN) was prepared from MgO and Nb_2O_5 mixed oxides, and calcined at 1100 °C, for 4 h. Then, following the batching formula, MN precursor was mixed with PbO and TiO_2, and

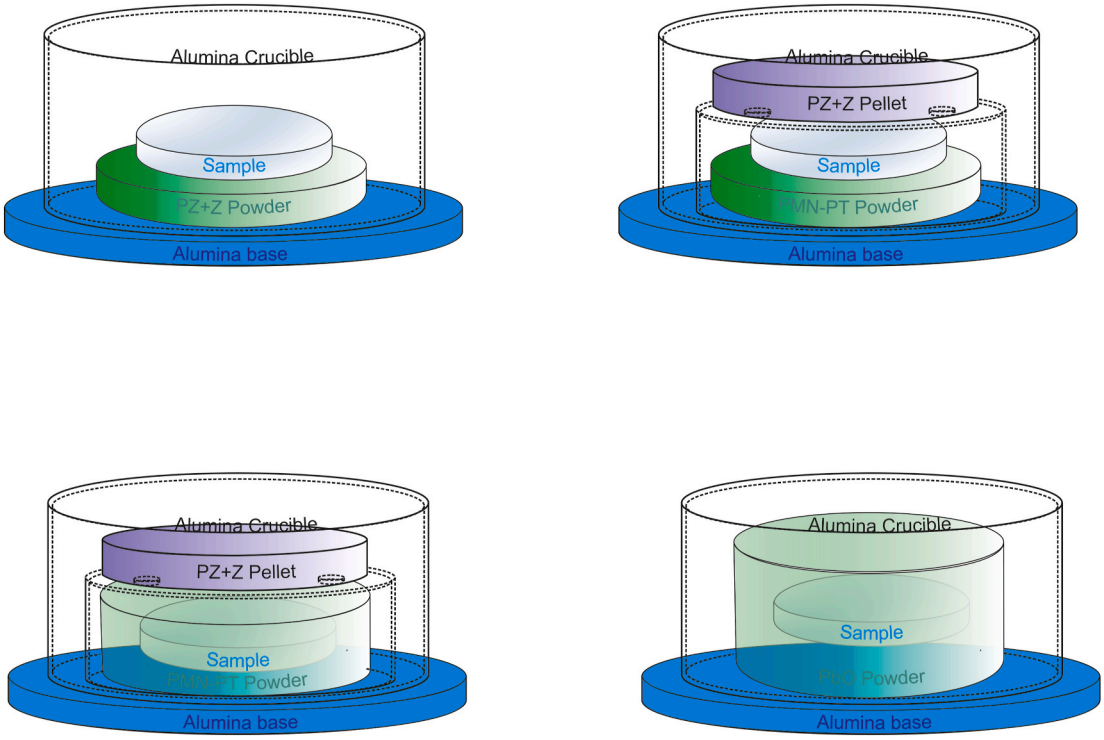

Fig. 2. Four distinct setup of bed powder and crucible applied for thermal treatment post sintering process: (a) PZ + Z powder bed and sealed crucible; (b) PMN-PT powder bed plus an inner crucible with holes with a pellet of PZ + Z on it and an outer sealed crucible; (c) sample covered by PMN-PT powder plus an inner crucible with holes with a pellet of PZ + Z on it and an outer sealed crucible; and (d) sample covered by PbO powder and sealed crucible.

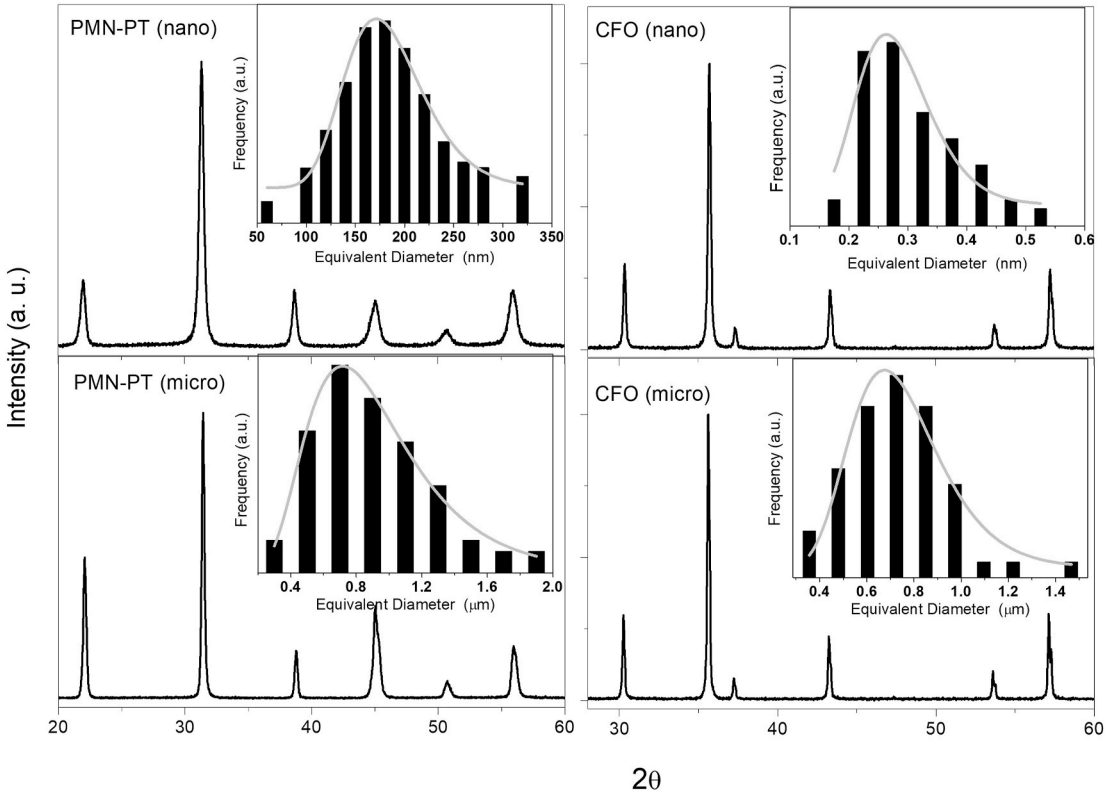

Fig. 3. XRD patterns and particle size distribution of PMN-PT and CFO powders with distinct average particle size.

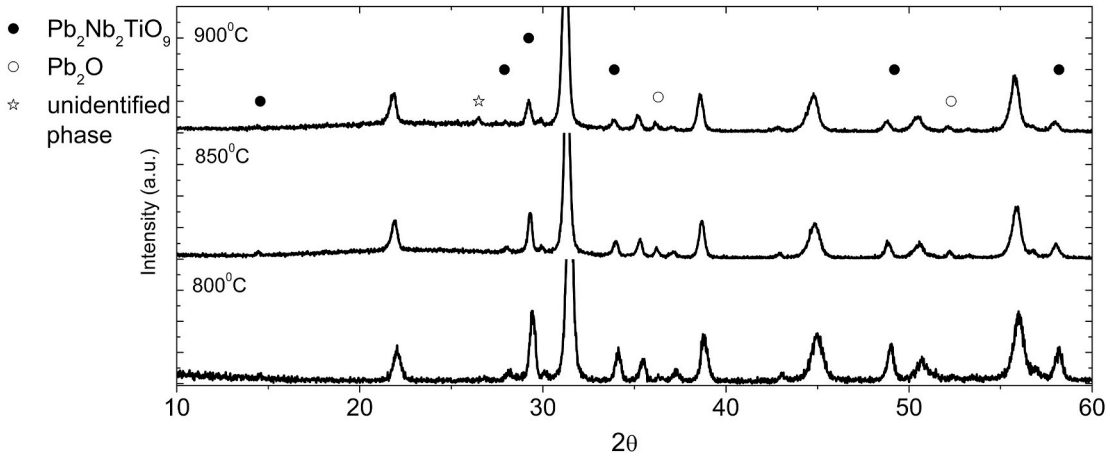

Fig. 4. XRD patterns of PMN-PT (nano)/CFO (nano) sintered at several temperatures using SPS sintering process. Phases peaks positions of secondary phases are indicated on the graphic.

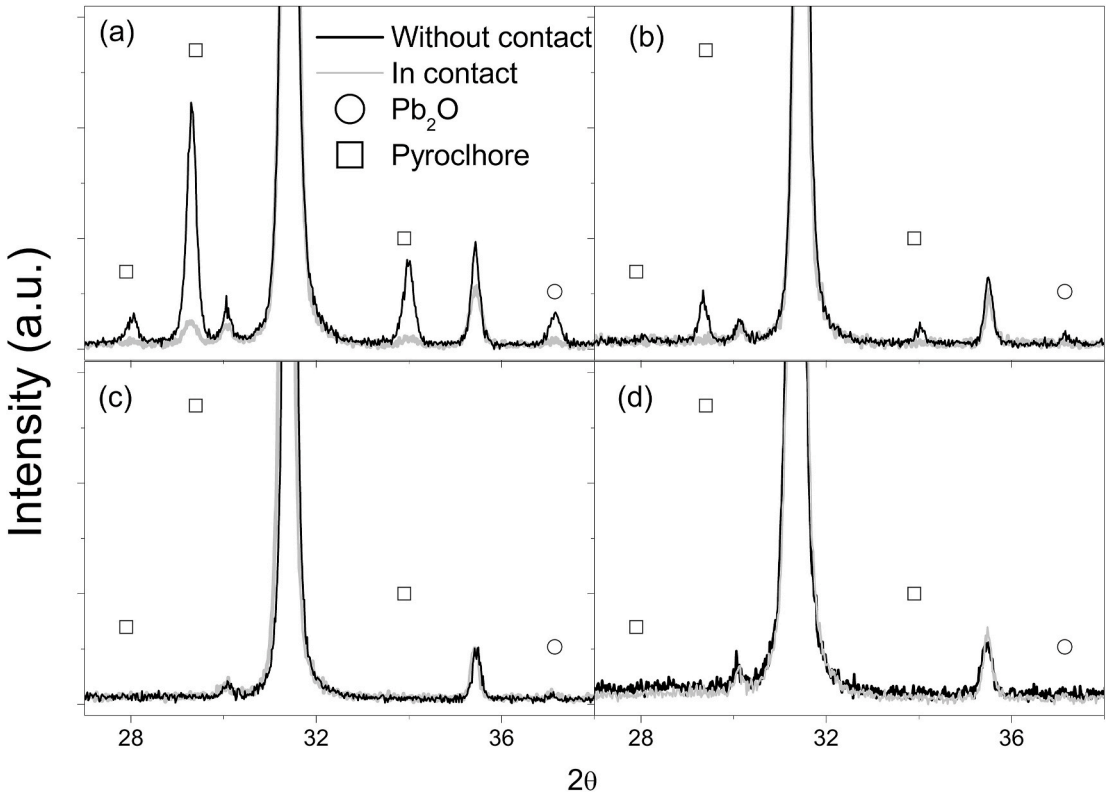

Fig. 5. XRD patterns of both polished surfaces of the pellets: (a) thermal treated for 6 h using setup presented in Fig. 2(a); (b) thermal treated for 10 h using setup presented in Fig. 2(b); thermal treated for 10 h using setup presented in Fig. 2(c); and (d) thermal treated for 10 h using setup presented in Fig. 2(d).

calcined at 900 °C, for 4 h, and ball milling grinded for 10 h. In order to reduce the particle size of the PMN-PT powder, ball milling with 1 mm diameter zirconia balls at 170 rpm was used for 24 h, followed by another 24 h with 0.5 mm balls.

To obtain four composites with different setup of grain size of PMN-PT and CFO, the powders of each phase were separated in two samples, one with smaller particle size and another with bigger particle size. The powders with smaller particle size were named PMN-PT (nano) and CFO (nano), the same process was adopted for powders with bigger particle size, resulting in PMN-PT (micro) and CFO (micro). At pairs these powders were blended at proportion of 80 and 20 mol %, within PMN-PT the powder with higher concentration, in a planetary ball mill (pulveriset PM200) at 300 rpm for 1 h with a ball-to-powder mass ratio of 1:1, resulting in 4 different mixture, each of these presenting distinct combination of particle size of each phase, as represented in Fig. 1.

Each powder mixture was sintered in Spark Plasma Sintering system using a Sinterer SPS-1020, Syntex, at different temperature for 300 s in argon atmosphere with heating and cooling ratio of 200 °C/minute and uniaxial pressure of 50 MPa. Sintering temperatures used for each powder combination are presented in Table 1. After sintering process, all samples were annealed for 24 h at 690 °C aiming to eliminate the carbon residues, secondary phases and oxidize, as previously reported by Viana et al. [28]. Moreover, this process was successful applied in many materials in order to eliminate the carbon resulted from SPS densification process [29,30] and in PMN-PT to remove secondary phases which resulted from SPS [12,28].

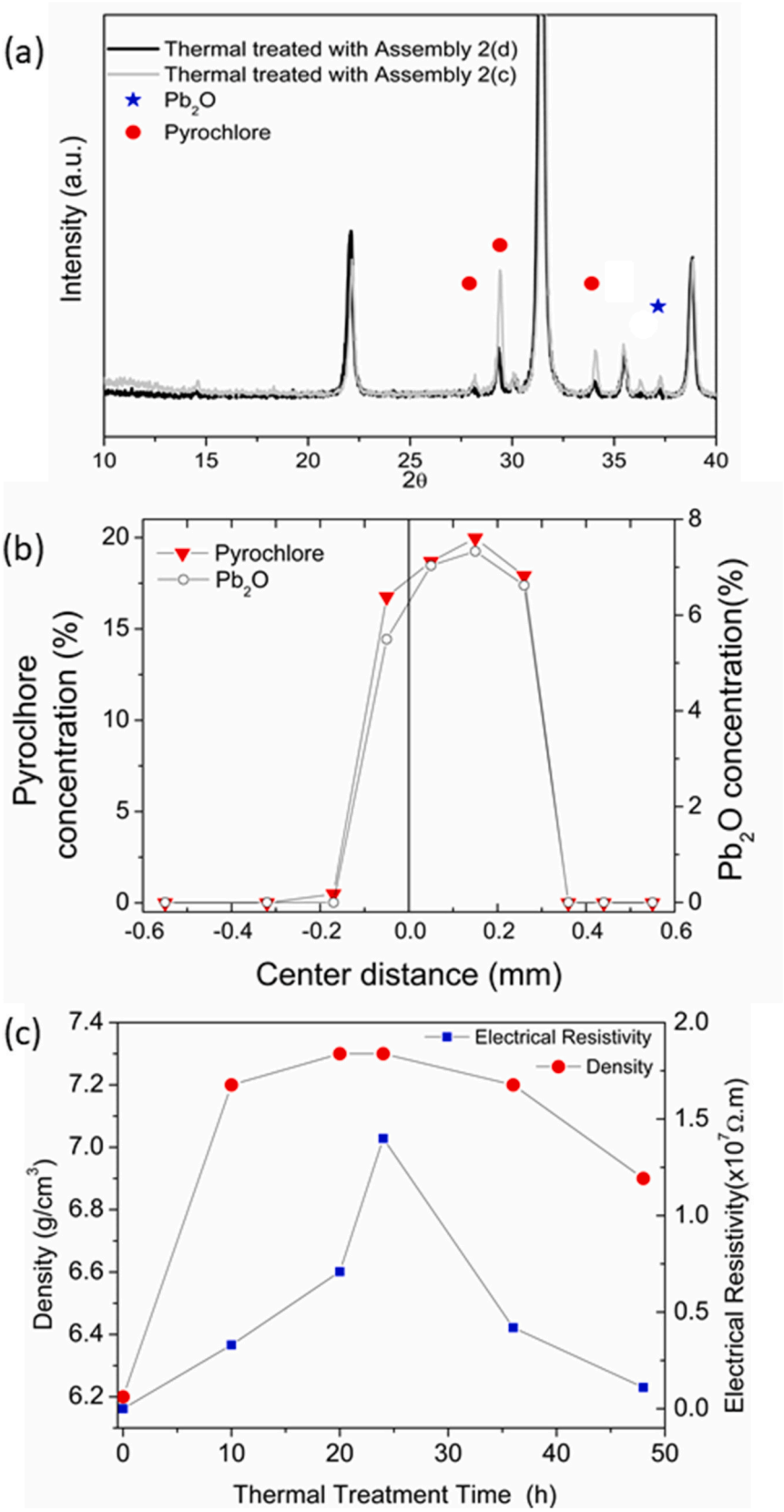

Fig. 6. (a) XRD patterns of samples thermal treated using set up presented in Fig. 2(c) and (d); (b) Secondary phase relative quantity in function of thickness of sample PMN-PT (nano)/CFO (nano) thermal treated for 10 h using set up 2(d); and (c) Relative density and dc electrical resistivity of PMN-PT (nano)/CFO (nano) thermal treated at different times using set up presented in Fig. 2 (d).

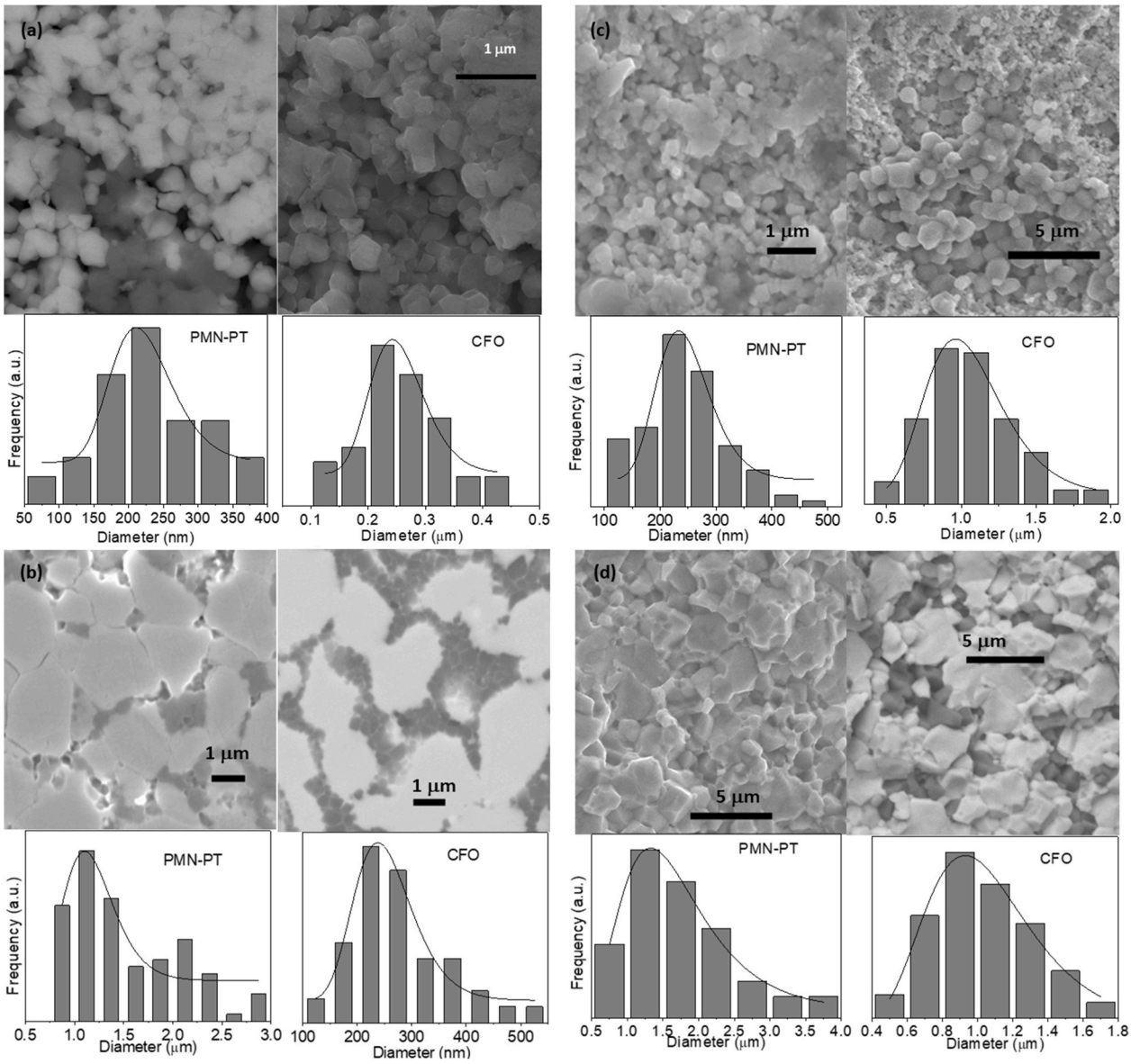

Fig. 7. Scanning electron microscopy (SEM) images and the grain size distribution for the different samples sintered by SPS and thermal treated for 24 h. (a) SEI and BEI image of same region of sample PMN-PT(nano)/CFO(nano); (b) SEI and BEI image of same region of sample PMN-PT(micro)/CFO(nano); (c) SEI image of two distinct region of sample PMN-PT(nano)/CFO(micro); and (d) SEI and BEI image of same region of sample PMN-PT (micro)/CFO(micro).

To perform thermal treatment after sintering process four setup of crucible (Fig. 2) were used. Similar procedures are already adopted in materials sintering with Pb in their composition with the goal to create a rich environment of PbO [31–33]. All applied setup are presented in Fig. 2: (a) powder bed of $PbZrO_3$ + 10% ZrO_2 (PZ + Z) and sealed crucible with PZ + Z; (b) powder bed of PMN-PT and sealed crucible with PZ + Z, the inner crucible has holes on top where was positioned a pellet of PZ + Z and all these setup were involved by another sealed crucible; (c) the pellet was completely involved by PMN-PT powder and sealed crucible with PZ + Z, the inner crucible has holes on top where was positioned a pellet of PZ + Z and all these setup were involved by another sealed crucible; and (d) the pellet was completely involved by PbO powder and sealed crucible with PZ + Z.

X-ray diffraction (XRD) analysis was performed using Rigaku Rotaflex RU200B diffractometer, with CuKα radiation. FullProff was applied in Rietveld Refinement. Particle size distribution was determined by a particle size analyzer Horiba CAPA-400. The electron microscope JEOL-JSM 5800 LV was used to examine morphology of the grains of the bulks. The average grain size of bulks were calculated using the log-normal distribution [34,35]. Electrical resistivity measurement was performed using an electrometer Keithley 617. Room temperature ferroelectric hysteresis loops were carried out with a modified Sawyer–Tower circuit at frequency of 50 Hz. The magnetic measurements were performed using Squid-VSM magnetometers by Quantum Design. Magnetoelectric coefficient was measured in the Physical Properties Measurement System (PPMS-6000). To perform magnetoelectric measurements at room temperature samples were electric poled at different electric field (Table 1). Distinct value electric field was applied on samples due to electric conductivity of the samples.

3. Results and discussion

Fig. 3 shows the room temperature X-ray diffraction patterns for PMN-PT powder after and before milling. The XRD patterns showed diffraction peaks corresponding to the perovskite phase of PMN-PT without a trace of another phase. Insets show the particle size distribution for each powder. The milled one has average particle size of 180 nm and another 850 nm. Fig. 3 also shows the room temperature X-ray

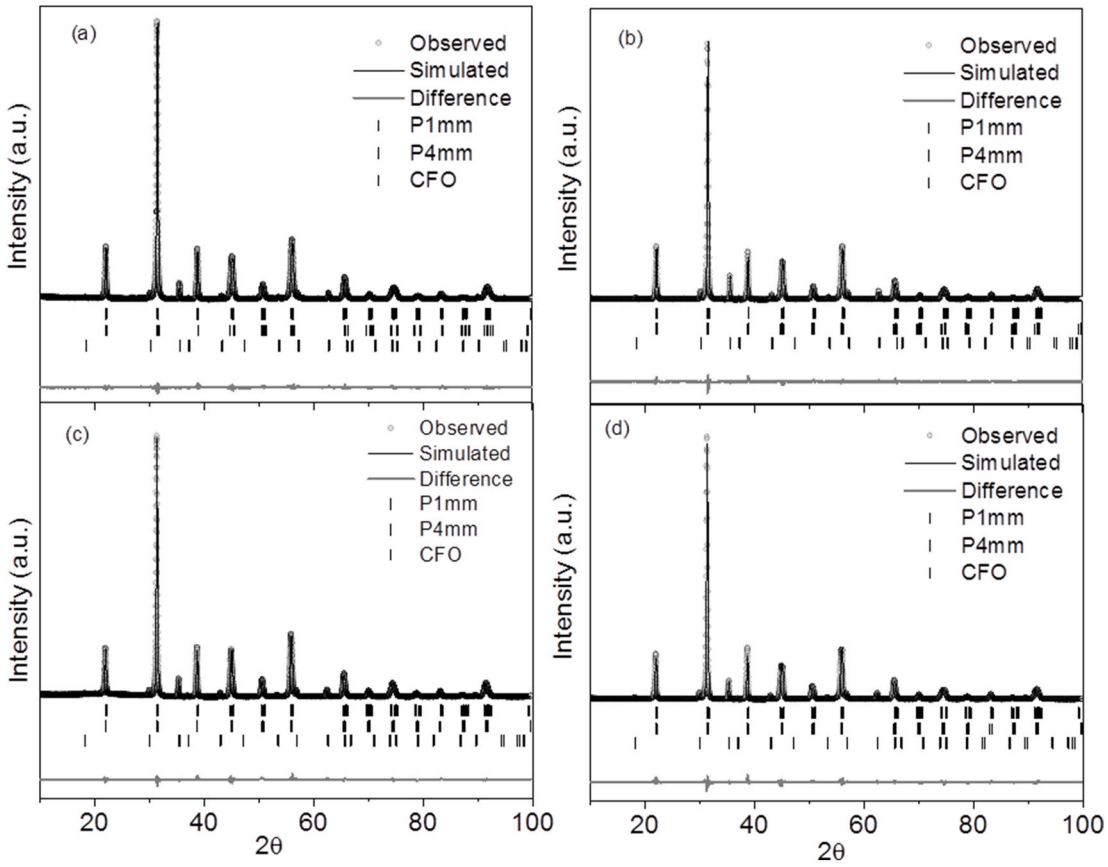

Fig. 8. Rietveld refinement of the XRD pattern of: (a) PMN-PT (nano)/CFO (nano); (b) PMN-PT (nano)/CFO (micro); (c) PMN-PT (micro)/CFO (nano); and (d) PMN-PT (micro)/CFO (micro).

Table 2
Ferroelectric quantity phase and chi square obtained by Rietveld method.

Phase quantity (%) Sample	P4mm (tetragonal)	P1m1 (monoclinic)	χ^2
PMN-PT (nano) CFO (nano)	25.8	74.2	2.0
PMN-PT (nano) CFO (micro)	25.2	74.8	3.1
PMN-PT (micro) CFO (nano)	57.5	42.5	2.1
PMN-PT (micro) CFO (micro)	52.4	47.6	4.8

diffraction patterns for CFO after and before thermal treatment. The XRD patterns showed the diffraction peaks corresponding phase of CFO. The powder thermal annealed presented average particle size of 800 nm while as prepared powder 270 nm.

PMN-PT and CFO powders were mixed and sintered at temperature according Table 1. The two composites containing PMN-PT (nano) were prepared at temperature of 800 °C while PMN-PT (micro)/CFO (nano) and PMN-PT (micro)/CFO (micro) were sintered at 900 °C and 950 °C, respectively. Distinct sintering temperature could be related with the fact that reducing particle size could modify the densification process by increasing the reactivity of particles, thus decreasing the sintering temperature [12,36,37]. All sintered composite presented high electrical dc conductivity (Table 1) compared with samples prepared by other methods [38,39].

On composites containing PMN-PT (nano) the sintering process induced appearance of secondary phases and low relative density, on the other hand ceramics containing PMN-PT (micro) presented only PMN-PT and CFO phases and high relative density (Table 1). Decreasing the average grain size of PMN-PT powder increased its reactivity leading to dissociation of PMN-PT phase in two secondary phases as observed by Jo el al [12]. Jo et al. reported the appearance of two secondary phases sintering PMN-PT with particle size of 9 nm using SPS, moreover the quantity of secondary phases observed were bigger than PMN-PT quantity phase [12]. CFO phase did not presented degradation after sintering process which could be related to the phase stability at temperatures applied [40].

Changing the sintering temperature did not prevent formation of secondary phases in composites containing PMN-PT (nano) as one can see in XRD in Fig. 4. This figure shows XRD patterns for distinct sintering temperature ranging from 800 °C to 900 °C, for a particular combination PMN-PT(nano)/CFO(nano). It has been observed additional phase $Pb_2Nb_2TiO_9$ (PDF 00-019-0692) and Pb_2O (PDF 00-002-0790) for all applied sintering temperature. At 900 °C an additional not identified phase appears showing that increasing the sintering temperature will result on more quantity of secondary phases. These phase formation arises from the dissociation of PMN-PT in a deficient Pb pyrochlore phase plus a phase rich in Pb, similar PMN-PT phase degradation was observed by Jo et al. [12] when the authors prepared PMN-PT using SPS technique. The selected sintering temperature to perform our studies was 800 °C due the fact that was the lower sintering temperature applied which avoid grain size growth. Aiming to remove secondary phases a thermal treatment was applied, thus four distinct crucible setup (Fig. 2) were tested only in PMN-PT (nano)/CFO (nano) pellet, ceramics containing PMN-PT (micro) did not presented phase degradation after sintering process.

Results of phase formation due changing the setup of crucible are

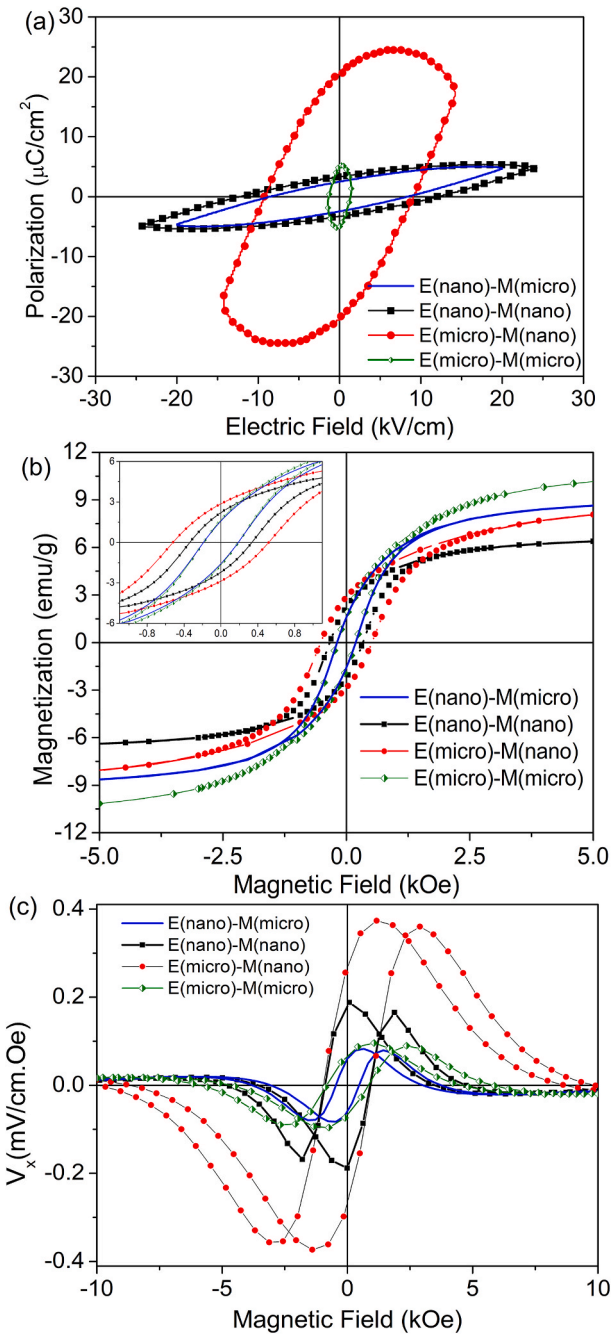

Fig. 9. Room temperature: (a) Polarization vs Electric Field; (b) Magnetization vs Magnetic Field; and (c) magnetoelectric coefficient vs magnetic field at frequency 1 kHz. The legend E refers to electric phase and M to magnetic phase.

discussed based in XRD patterns presented in Fig. 5. Fig. 5 (a) shows XRD results for a sample thermal treated for 6 h applying the setup represented in Fig. 2 (a). One can see the decrease of secondary phase quantity in comparison with that sample without thermal treatment presented in Fig. 4. However, the face which was in contact with PZ + Z bed powder showed less quantity of secondary phases than the another surface without contact, demonstrating that the contact of sample and PZ + Z powder play a role on the task of eliminating undesirable impurities. Several studies on Pb based ferroelectrics had demonstrated that bed powder has a play controlling the Pb losses on sintering process [31–33].

The setup presented in Fig. 2 (b) were applied in thermal treatment for 10 h, however bed powder were made of PMN-PT powder instead of PZ + Z powder. This setup was more efficient on eliminating at secondary phase compared with set up 2 (a). However, it was not possible to eliminate completely them at these conditions. Besides, distinct results were obtained on each surface, showing that the bed powder contact with sample play a role on this action.

Both set up presented in Fig. 2 (c) and 2 (d) were applied on a thermal treatment for 10 h. Both cases no secondary phases were observed at surface. However, cracking the sample and make it on powder, phases $Pb_2Nb_2TiO_9$ and Pb_2O are still detected by XRD, Fig. 6 (a). Between these two samples, the sample thermal treated using set up 2 (d) presented less quantity of secondary phases than sample thermal treated with 2(c).

Sample thermal treated using setup 2 (d) was used to investigate the quantity of secondary phases inside the sample. To estimate the relationship of phase quantity of $Pb_2Nb_2TiO_9$ and Pb_2O inside, it was used the intensity value of the most intense peak of each phase. Thus, the phase concentration was estimated by the ratio of the secondary phase peak intensity to the sum of all other phases peak intensity (PMN-PT + $Pb_2Nb_2TiO_9$ + Pb_2O + CFO). Calculating the relationship of peak intensity of XRD, a qualitative analysis of concentration of secondary phases was obtained and presented on Fig. 6 (b). According to the distance of bulk's center it was observed that the reaction of $Pb_2Nb_2TiO_9$ + Pb_2O + PbO (atmosphere created by crucible setup) = PMN-PT occurs from outside to inside.

Thermal treatment using the setup presented in Fig. 2(d) was applied for different times varying from 0 to 36 h. Sample thermal treated for 24 h exhibits higher values of density and dc electrical resistivity (Fig. 6(c) and Table 1). The same protocol was applied to other three samples increasing values of density and electrical resistivity (Table 1). Besides, secondary phases were eliminated of sample PMN-PT(nano)/CFO (micro). For longer thermal treatments times both value of relative density and electrical resistivity decrease for all samples due to the losses of PbO.

Fig. 7 shows the scanning electron microscopy (SEM) images and the grain size distribution for the different samples sintered by SPS, average grain size for each sample and each phase are shown in Table 1. Fig. 7 (a), 7(b) and 7(d) presents the same bulk region for PMN-PT(nano)/CFO (nano), PMN-PT(micro)/CFO(nano) and PMN-PT(micro)/CFO(micro), respectively, presenting on the left side Secondary electron imaging (SEI) and on the right side the Backscattered electron imaging (BEI). On BEI image brighter grains represents PMN-PT and darker grains CFO. For PMN-PT(nano)/CFO(nano) the of grain size distribution of both phases is similar, thus the average grain size of two phase is close. By micrography of PMN-PT(micro)/CFO(nano), Fig. 7(b), is notable that the grain size of PMN-PT is bigger than 1 μm and CFO grain size is smaller than the PMN-PT reaching up to 500 nm. The same situation is observed in PMN-PT(micro)/CFO(micro), however on this sample CFO grain size is bigger than the PMN-PT(micro)/CFO(nano). Fig. 7(c) shows two distinct region of same sample PMN-PT (nano)/CFO(micro), on the left image is possible to see mostly grains of PMN-PT(nano) while at right micrography is shown the difference of grain size between the phases.

Table 1 presents average grain size for each phase and pooling field for samples thermal treated for 24 h. In addition others information are shown in Table 1 like relative density and apparent density for samples thermal treated for 0, 24 and 36 h.

Setup presented in 2(d) was applied for 24 h in all samples in order to investigate theirs properties. Fig. 8 shows room temperature X-ray diffraction patterns at the room temperature and Rietveld refinament for (0.8) [0.675 PMN - 0.325 PT]/(0.2) CFO with distinct grain size configuration. For all the samples XRD patterns showed the diffraction peaks corresponding to the phase of CFO and perovskite phase of PMN-PT without a trace of secondary phase. Table 2 shows the tetragonal and monoclinic phase quantity obtained by Rietveld Refinament. Lowest values of chi square where obtained for samples presenting simultaneously tetragonal and monoclinic phase, it is well-known that this

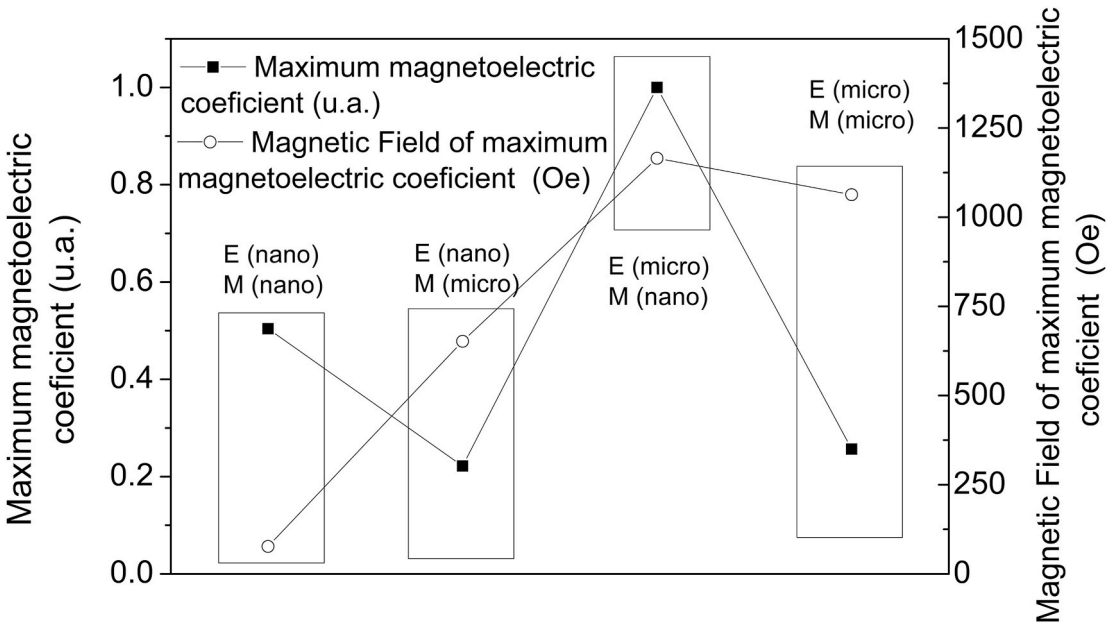

Fig. 10. Value of maximum magnetoelectric coefficient and magnetic field intensity where the maximum magnetoelectric coefficient was observed for distinct configurations of average grain size. The legend E refers to electric phase and M to magnetic phase. The plotted line is a guide for the eye.

composition of PMN-PT lies in the morphotropic phase boundary [41]. It was observed the dependence of PMN-PT crystal structure with grain size, as well as was already reported for 0.7 PMN – 0.3 PT [12]. When the grain size was reduced the quantity of monoclinic phase increase whiles the quantity of tetragonal phase decrease, as one can see on Table 2. The transition of a distorted structure to a more symmetrical structure by reducing the grain size was observed in several ferroelectric materials like $BaTiO_3$ [42] and PMN-PT [12,13].

By Fig. 9 (a), polarization curve vs electric field, it is possible to see that the grain size of electrical phase (E) determine the behavior of these curves. Samples containing PMN-PT (nano) presented a slim loop characteristic while the others with PMN-PT (micro) displayed a conductive behavior. Also samples containing PMN-PT (micro) presented leakage current at low values of electric field, smaller than that observed on bulks containing PMN-PT (nano), therefore small values of applied electric field was achieved during electric pooling process of these samples. Specifically, the sample PMN-PT (micro)/CFO (micro) display a conductivity behavior, thus at this sample only 0.3 kV/cm of electric field during electric polarization process could be applied (Table 1). The influence of grain downsizing of ferroelectric phase showed increase of electrical resistivity and smaller values of electrical polarization. The decrease of electrical polarization could be related with type and configuration of ferroelectrics domains which depends of crystal symmetry which was modified by downsizing the grain size [13].

Fig. 9(b) shows the magnetization vs. magnetic field curve at room temperature. Samples with CFO (micro) presented smaller value of coercive field and remanent magnetization than that observed in CFO (nano). This behavior is in agreement with reported for magnetic materials [19,20,40], since that the increase on grain size results in smaller coercive field. Samples containing CFO(micro) showed same behavior on magnetization for magnetic fields up to 0.4 KOe while on samples containing CFO(nano) was observed distinct response which could be originated by stress of PMN-PT phase. The influence of PMN-PT phase in magnetic properties also could be observed on remanent magnetization and coercive field in samples with CFO (nano), Fig. 9(b). Due the fact that the stress in CFO results in increase of coercive field [43] it is possible that the difference observed in coercive field and remanent magnetization maybe have originated of stress of PMN-PT on CFO.

One can see the self-biased effect (SE) in all samples (Fig. 9(c)), i.e., magnetoelectric response in zero magnetic bias field [2]. The origin of this effect is the stress which one phase exerts against another. Besides, the SPS has influence in the generation of this effect, since that the SE was not observed on the similar compositions of PMN-PT/CFO prepared by other methods like hot pressing [44], conventional sintering process [38,45,46]. The SPS create an intrinsic strain due the high rates of temperature changes and the pressure applied during the sintering process.

Fig. 10 shows the values of normalized maximum of coefficient magnetoelectric and the intensity of magnetic field where this response was measured for all samples. Regarding the maximum value of the magnetoelectric coefficient, analyzing the two composites with the average size of grain of ferroelectric phase (nano), recalling that were polarized in the same condition, one can see that sample with ferrite phase (nano) has a higher coefficient value than that with ferrite phase (micro), as expected based on Yue theoretical model [22]. Comparing at composites with ferroelectric phase (micro), though compromised by the high electrical conductivity harming the process of polarization, it's possible to note that composite with CFO (nano) presents higher value of magnetoelectric coefficient. Moreover, the highest coefficient was observed in PMN-PT (micro)/CFO (nano) which is in agreement with the proposed model in Ref. [22], where is expected maximum value of magnetoelectric coefficient when the average grain size of ferroelectric phase is on the micrometer order and magnetic phase has a size of few hundred nanometers. It was also noticed that the magnetic field in which it is obtained the maximum value of the magnetoelectric coefficient in samples with PMN-PT (nano) are lower when compared to with PMN-PT (micro).

Besides, it is possible to note that decreasing ferrite grain size also decrease the value of the magnetic field where the maximum of magnetoelectric is observed as well as ferroelectric phase, leading to a self-biased behavior. Thus, composite that requires smallest bias magnetic field to the coefficient reaches its maximum value, is the PMN-PT (nano)/CFO (micro) and the one with highest coefficient is the PMN-PT (micro)/CFO (nano).

4. Conclusions

Samples of magnetoelectric composites 0.8 (PMN-PT)/0.2 (CFO) with distinct configuration of grain size of ferroelectric and magnetic phases were prepared without presence of any secondary phase. A

protocol of thermal treatment post sintering aiming to eliminated secondary phases and improve electrical resistivity and density was established. Electric and magnetic hysteresis loops showed the existence of electric and magnetic order and the magnetoelectric measurements confirms the coupling between them. The electric and magnetic properties showed dependence with grain size of individual phases, for example by the fact of observing that the presence of PMN-PT (nano) and (micro) in samples with CFO (nano) results in distinct magnetic response. The difference on magnetic properties could be generated by stress of PMN-PT under CFO. In coupled properties, it was noticed that all composites showed self-biased effect on the magnetoelectric coefficient. Besides, the sample with smallest grain size of both phases showed the maximum coefficient magnetoelectric at lowest magnet field. Meanwhile, conclusions about the influence of microstructure on the magnetoelectric coefficient, particularly the effect of self-biased effect are still under investigation.

Declaration of competing interest

The authors declare that they have no known competing financial interests or personal relationships that could have appeared to influence the work reported in this paper.

Acknowledgements

To Mr. Francisco J. Picon (GCFerr), Mrs. Natália Ap. Zanardi (DF-UFSCar). To FAPESP (Proc. n. 2008/04025-0), CAPES (Aux. n.:3012/2014) and CNPq (Proc. n. 407547/2013-4) for the financial support.

References

[1] R. Adnan Islam, S. Priya, Progress in dual (Piezoelectric-Magnetostrictive) phase magnetoelectric sintered composites, Adv. Condens. Matter Phys. (2012) 2012.
[2] Y. Zhou, D. Maurya, Y. Yan, G. Srinivasan, E. Quandt, S. Priya, Self-biased magnetoelectric composites: an overview and future perspectives, Energy Harvest. Syst. 3 (2016) 1–42.
[3] N.A. Hill, Why are there so few magnetic ferroelectrics? J. Phys. Chem. B 104 (2000) 6694–6709.
[4] M.M. Vopson, Fundamentals of multiferroic materials and their possible applications, Crit. Rev. Solid State Mater. Sci. (2015) 1–28.
[5] C.-W. Nan, M. Bichurin, S. Dong, D. Viehland, G. Srinivasan, Multiferroic magnetoelectric composites: historical perspective, status, and future directions, J. Appl. Phys. 103 (2008) 1.
[6] Y. Zhou, D. Maurya, Y. Yan, G. Srinivasan, E. Quandt, S. Priya, Self-Biased Magnetoelectric Composites: an Overview and Future Perspectives, Energy Harvesting and Systems, 2016.
[7] S.C. Yang, C.S. Park, K.H. Cho, S. Priya, Self-biased magnetoelectric response in three-phase laminates, J. Appl. Phys. 108 (2010).
[8] S.C. Yang, C.W. Ahn, K.H. Cho, S. Priya, Self-bias response of lead-free (1-x)[0.948 K0.5Na0.5NbO3-0.052 LiSbO3]-xNi(0.8)Zn(0.2)Fe(2)O(4)-nickel magnetoelectric laminate composites, J. Am. Ceram. Soc. 94 (2011) 3889–3899.
[9] B.-S. Kang, D. Gu-Choi, S.-K. Choi, Effects of grain size on pyroelectric and dielectric properties of Pb0. 9La0. 1TiO3 ceramics, J. Mater. Sci. Mater. Electron. 9 (1998) 139–144.
[10] H. Martirena, J. Burfoot, Grain-size effects on properties of some ferroelectric ceramics, J. Phys. C Solid State Phys. 7 (1974) 3182.
[11] S. Choudhury, Y. Li, C. Krill, L. Chen, Effect of grain orientation and grain size on ferroelectric domain switching and evolution: phase field simulations, Acta Mater. 55 (2007) 1415–1426.
[12] W. Jo, T.-H. Kim, D.-Y. Kim, S.K. Pabi, Effects of grain size on the dielectric properties of Pb (Mg1/3Nb2/3) O3-30 mol% PbTiO3 ceramics, J. Appl. Phys. 102 (2007), 074116.
[13] Z.-G. Ye, Handbook of Advanced Dielectric, Piezoelectric and Ferroelectric Materials: Synthesis, Properties and Applications, Elsevier, 2008.
[14] K. Vasundhara, S.N. Achary, S.K. Deshpande, P.D. Babu, S.S. Meena, A.K. Tyagi, Size dependent magnetic and dielectric properties of nano CoFe2O4 prepared by a salt assisted gel-combustion method, J. Appl. Phys. 113 (2013).
[15] B.G. Toksha, S.E. Shirsath, S.M. Patange, K.M. Jadhav, Structural investigations and magnetic properties of cobalt ferrite nanoparticles prepared by sol-gel auto combustion method, Solid State Commun. 147 (2008) 479–483.
[16] K. Maaz, A. Mumtaz, S.K. Hasanain, A. Ceylan, Synthesis and magnetic properties of cobalt ferrite (CoFe2O4) nanoparticles prepared by wet chemical route, J. Magn. Magn Mater. 308 (2007) 289–295.
[17] Y.I. Kim, D. Kim, C.S. Lee, Synthesis and characterization of CoFe2O4 magnetic nanoparticles prepared by temperature-controlled coprecipitation method, Physica B 337 (2003) 42–51.
[18] J. Mohapatra, A. Mitra, D. Bahadur, M. Aslam, Superspin glass behavior of self-interacting CoFe 2 O 4 nanoparticles, J. Alloys Compd. 628 (2015) 416–423.
[19] T. Gaudisson, M. Artus, U. Acevedo, F. Herbst, S. Nowak, R. Valenzuela, S. Ammar, On the microstructural and magnetic properties of fine-grained CoFe2O4 ceramics produced by combining polyol process and spark plasma sintering, J. Magn. Magn Mater. 370 (2014) 87–95.
[20] B.D. Cullity, C.D. Graham, Introduction to Magnetic Materials, John Wiley & Sons, 2011.
[21] R.A. Islam, S. Priya, Effect of piezoelectric grain size on magnetoelectric coefficient of Pb (Zr0. 52Ti0. 48) O3–Ni0. 8Zn0. 2Fe2O4 particulate composites, J. Mater. Sci. 43 (2008) 3560–3568.
[22] Y. Yue, K. Xu, T. Chen, E. Aifantis, Size effects on magnetoelectric response of multiferroic composite with inhomogeneities, Phys. B Condens. Matter 478 (2015) 36–42.
[23] A. Gualdi, F. Zabotto, D. Garcia, A. De Oliveira, Stress magnetization model for magnetostriction in multiferroic composite, J. Appl. Phys. 114 (2013), 053913.
[24] M. Sade, F. de Castro Bubani, F. Lovey, V. Torra, Effect of grain size on stress induced martensitic transformations in a Cu–Al–Be polycrystalline shape-memory alloy. Pseudoelastic cycling effects and microstructural modifications, Mater. Sci. Eng., A 609 (2014) 300–309.
[25] A. Bhattacharjee, S. Bhargava, V. Varma, S. Kamat, A. Gogia, Effect of β grain size on stress induced martensitic transformation in β solution treated Ti–10V–2Fe–3Al alloy, Scripta Mater. 53 (2005) 195–200.
[26] T. Hungria, J. Galy, A. Castro, Spark plasma sintering as a useful technique to the nanostructuration of piezo-ferroelectric materials, Adv. Eng. Mater. 11 (2009) 615–631.
[27] R. Chaim, M. Levin, A. Shlayer, C. Estournès, Sintering and densification of nanocrystalline ceramic oxide powders: a review, Adv. Appl. Mater. 107 (2008) 159–169.
[28] D.S.F. Viana, J.A. Eiras, W.J. Nascimento, F.L. Zabotto, D. Garcia, Controlled Atmosphere Thermal Treatment for Pyrochlore Phase Elimination of PMN-PT/CFO Prepared by Spark Plasma Sintering, Advanced Materials Research, Trans Tech Publ, 2014, pp. 274–279.
[29] M. Zhu, J. Tang, N. Ke, Q. Qiu, N. Lei, Y. Hou, H. Yan, J. Xu, Annealing effect on relaxor behaviours of spark plasma sintered Pb (Sc1/2Nb1/2) O3 superfine ceramics, Adv. Appl. Mater. 110 (2011) 74–79.
[30] D.V. Dudina, A.K. Mukherjee, Reactive spark plasma sintering: successes and challenges of nanomaterial synthesis, J. Nanomater. (2013) 5, 2013.
[31] M. Safar, T.W. Button, M. Zabcik, Control of PbO Loss during Sintering of PZT: Laboratory vs Industry, 2017 Joint IEEE International Symposium on the Applications of Ferroelectric (ISAF)/International Workshop on Acoustic Transduction Materials and Devices (IWATMD)/Piezoresponse Force Microscopy (PFM), IEEE, 2017, pp. 83–88.
[32] A.I. Kingon, J.B. Clark, Sintering of PZT ceramics: I, atmosphere control, J. Am. Ceram. Soc. 66 (1983) 253–256.
[33] K. Härdtl, H. Rau, PbO vapour pressure in the Pb (Ti1−x) O3 system, Solid State Commun. 7 (1969) 41–45.
[34] M.F. Vaz, M. Fortes, Grain size distribution: the lognormal and the gamma distribution functions, Scripta Metall. 22 (1988) 35–40.
[35] W. Fayad, C. Thompson, H. Frost, Steady-state grain-size distributions resulting from grain growth in two dimensions, Scripta Mater. 40 (1999) 1199–1204.
[36] L.J. Wang, X. Yang, X.J. Liu, Z. Jiao, Z.R. Huang, Effects of Particle Size on Densification Behavior of Si3N4 Ceramics, Key Engineering Materials, Trans Tech Publ (2016) 182–187.
[37] S. Diouf, A. Molinari, Densification mechanisms in spark plasma sintering: effect of particle size and pressure, Powder Technol. 221 (2012) 220–227.
[38] F. Zabotto, A. Gualdi, P. de Camargo, A. de Oliveira, J. Eiras, D. Garcia, Grain coarsening and its effects on the properties of magnetoelectric 0.675 (Pb (Mg1/3Nb2/3) O3)–0.325 PbTiO2/CoFe2O4 particulate composites, J. Alloys Compd. 676 (2016) 80–85.
[39] C.P.F. Perdomo, R.H.A. Kiminami, D. Garcia, Microwave assisted sintering of nanocristalline PMN-PT/CoFe2O4 prepared by rapid one pot pechini synthesis: dielectric and magnetoelectric characteristics, Ceram. Int. 45 (2019) 7906–7915.
[40] K. Venkata Siva, S. Sudersan, A. Arockiarajan, Bipolar magnetostriction in CoFe2O4: effect of sintering, measurement temperature, and prestress, J. Appl. Phys. 128 (2020) 103904.
[41] M. Sepliarsky, R.E. Cohen, First-principles based atomistic modeling of phase stability in PMN–xPT, J. Phys. Condens. Matter 23 (2011) 435902.
[42] M. Frey, D. Payne, Grain-size effect on structure and phase transformations for barium titanate, Phys. Rev. B 54 (1996) 3158.
[43] L. Zhao, Q. Jiang, Effects of applied magnetic field and pressures on the magnetic properties of nanocrystalline CoFe 2 O 4 ferrite, J. Magn. Magn Mater. 322 (2010) 2485–2487.
[44] A.J. Gualdi, F.L. Zabotto, D. Garcia, A.S. Bhalla, R. Guo, P.C. de Camargo, A.J.A. de Oliveira, Dynamic magnetization on the low temperature magnetoelectric effect in multiferroic composites, J. Phys. Condens. Matter 30 (2018) 325803.
[45] Y. Pei, Q. Li, W. Shi, B. Zhang, Q. Chen, X. Yue, D. Xiao, J. Zhu, Effect of CoFe2O4 content on the dielectric and magnetoelectric properties in CoFe2O4/Pb (Mg1/3Nb2/3) 0.35 Ti0. 65O3 composites, Ferroelectrics 410 (2010) 82–87.
[46] A.D. Sheikh, A. Fawzi, V. Mathe, Microstructure–property relationship in magnetoelectric bulk composites, J. Magn. Magn Mater. 323 (2011) 740–747.